

# Robust ion current oscillations under a steady electric field: An ion channel analog

Yu Yan,<sup>1</sup> Yunshan Wang,<sup>1</sup> Satyajyoti Senapati,<sup>1</sup> Jarrod Schiffbauer,<sup>2</sup> Gilad Yossifon,<sup>3</sup> and Hsueh-Chia Chang<sup>1,\*</sup>

<sup>1</sup>Department of Chemical and Biomolecular Engineering, University of Notre Dame, Notre Dame, Indiana 46556, USA

<sup>2</sup>Department of Aerospace and Mechanical Engineering, University of Notre Dame, Notre Dame, Indiana 46556, USA

<sup>3</sup>Faculty of Mechanical Engineering, Micro- and Nanofluidics Laboratory, Technion-Israel Institute of Technology, Technion City 32000, Israel

(Received 9 April 2016; published 26 August 2016)

We demonstrate a nonlinear, nonequilibrium field-driven ion flux phenomenon, which unlike Teorell's nonlinear multiple field theory, requires only the application of one field: robust autonomous current-mass flux oscillations across a porous monolith coupled to a capillary with a long air bubble, which mimics a hydrophobic protein in an ion channel. The oscillations are driven by the hysteretic wetting dynamics of the meniscus when electro-osmotic flow and pressure driven backflow, due to bubble expansion, compete to approach zero mass flux within the monolith. Delayed rupture of the film around the advancing bubble cuts off the electric field and switches the monolith mass flow from the former to the latter. The meniscus then recedes and repairs the rupture to sustain an oscillation for a range of applied fields. This generic mechanism shares many analogs with current oscillations in cell membrane ion channel. At sufficiently high voltage, the system undergoes a state transition characterized by appearance of the ubiquitous  $1/f$  power spectrum.

DOI: [10.1103/PhysRevE.94.022613](https://doi.org/10.1103/PhysRevE.94.022613)

## I. INTRODUCTION

Onsager was able to show from considerations of microscopic reversibility that the near-equilibrium, linear-response transport tensor for coupled fluxes driven by appropriate potential gradients is symmetric [1]. However, such linear, open-flux systems cannot exhibit oscillations under steady forcing by a single applied gradient, being essentially reduced to a one-dimensional (1D) flow in phase space. This observation is obviously contradicted by the oscillatory ion currents through the ion channels of a single cell [2], which must then operate at a highly nonlinear regime beyond Onsager's linear response theory. While Onsager reciprocity extends to nonlinear response [3–5], the requisite nonlinearity for autonomous oscillations such as occur in a transmembrane ion channel is still under debate. Field dependence of the conformation of the gating proteins on the electric field [6], oscillating water vapor and liquid states in the channel [7], competition between hydrated ammonia gas and water in the pores [8,9], and switching between hydrophobic glycerol facilitators and hydrophilic aquaporins [10] have all been proposed for different cells and protein pores. Such ion channel oscillations are very robust and occur for all potential jumps across the cell. A strong electro-osmotic flow through the phloem tissue in leaves [11] and alpha-hemolysin pores of staphylococcal [12] have been shown to significantly contribute to both ion and neutral solute transport through transmembrane pores, even large ones that are only weakly ion selective. Mass, current, and electric field fluxes can hence all be coupled in a nonlinear manner to produce the oscillations. The possibility of water vapor or ammonia gas in ion channels may be analogous to the role of water vapor in the present device, even though the liquid-vapor interface in a confined channel is unlikely to exhibit changes of curvature. However, the highly nonlinear wetting and dewetting contact line dynamics of film rupture

and drop formation [13,14]—themselves having a nonlinear electrokinetic component [15]—likely contribute to oscillations. Together, these suggest new nonlinear mechanisms, other than hysteretic gating protein conformation changes, that have yet to be thoroughly explored. Furthermore, joule heating of the thin film can also introduce additional nonlinearities, including Marangoni-like convective instabilities [16], as well as shifting the liquid-vapor equilibrium inside the bubble. Based on the behavior of other nonlinear systems [17], it is reasonable to suppose noisy fluctuations, for instance, due to interfacial instabilities, may play an important role in the transition corresponding to the appearance of the  $1/f$  response reported herein.

Teorell [18] first showed experimentally that ion and mass flux through a charged channel can be oscillatory if the three steady macroscopic gradients are imposed in specific directions: pressure, electric potential, and ionic strength. Meares and Page carried out complementary experimental and theoretical studies of membrane oscillations operating in a galvanostatic mode [19,20]. Kobatake and Fujita [21] and Rubinstein [22] then showed that the key mechanism for the Teorell oscillation is due to the nonlinearity from the electro-osmotic flow dependence on the local ion concentration, such that the fluid flow direction is multivalued with the same concentration drop. The ion current can also be multivalued (hysteretic) with respect to the applied voltage, due to a combination of pressure-driven and electro-osmotic flow effects on the ion flux, and switching between the two locally stable states can be achieved with properly oriented macroscopic pressure and concentration gradients. Later, Patushenko demonstrated a potentiostatic mode of oscillation [23,24]. This mechanism was given further detailed study by Abu-Rjal *et al.* [25], who showed that the concentration gradient does not need to be imposed externally but can occur spontaneously by field-induced ion depletion at one membrane surface to introduce a concentration polarization across the membrane. Such ion concentration polarization occurs only beyond a threshold voltage and is difficult to sustain in a crowded cellular

\*Corresponding author: hchang@nd.edu

environment. Although multiple gradients in the required directions do exist across biological cell membranes, the Donnan potential gradient and the osmotic pressure gradient are established by the ionic strength gradient to establish thermodynamic equilibrium—they are not externally imposed gradients. Also, for highly selective small pores, the intrapore ionic strength and its effect on the pore electro-osmosis is independent of the external concentration gradient [26]. The multiple gradient mechanism hence cannot be responsible for the robust oscillations in the ion channels.

Nonlinear ion transport phenomena, both the oscillatory and nonoscillatory variety, through a nanoporous ion-selective medium due to just a potential gradient have attracted considerable attention recently because of the advent of nanopore molecular sensing [27] and rapid sequencing [28]. Both empty pores and pores loaded with proteins or ion-channel proteins have been used for this next-generation molecular sensing-characterization technologies. Both internal and external nonlinear flow and current resistance due to concentration and charge polarization and a microvortex instability have been predicted and verified [25,29]. Most relevantly, flow effects like in Teorell oscillations have been shown to change the nonlinear ion flux [30]. dc current rectification and inversion have been observed and analyzed [26,31]. Water splitting across a bipolar membrane can dramatically alter the local pH [32] and this pH actuation may be responsible for hysteretic gating conformation dynamics with respect to pH [11]. Precipitation assisted ion current oscillations have been observed in nanopores with only a potential gradient [33], where reversible precipitation offers the required nonlinear mechanism. However, such oscillations only occur under very specific conditions conducive for reversible ion precipitation and are hence not related to ion channel oscillations.

In this article, we report a robust oscillatory ion-mass flux phenomenon in a coupled porous medium-capillary system under just a potential gradient that shares many analogs with ion channel oscillations. Instead of a gating protein, we introduce an air-liquid meniscus in the capillary whose film thickness and conductance (hence the electro-osmotic flow of the system) both exhibit hysteretic dependence on the electric field, like the conformation and osmotic pressure of a gating protein. Instead of relying on the ionic strength dependence of electroosmosis, as in Teorell's theory, we rely on electric field dependence to remove the need for a concentration gradient. The air-liquid interface mimics the boundary surface between hydrophobic and hydrophilic regions of a protein [10] or actual interfaces between water gas-liquid states [7] or between ammonia and water [8] with nonlinear dewetting-wetting dynamics and film rupture of the advancing bubble. The porous medium provides a unique mechanism to create the oscillation and render it ubiquitous for all negative electric fields (i.e., to the left in Fig. 1). The silica monolith has large pores with non-negligible surface charge in aqueous solution. So, much like phloem plant tissues or water channels, while it can sustain both the electro-osmotic and pressure-driven flows required for multiple gradient theories [18,21], it is not, however, strongly ion selective. The oscillatory response here is robust because the flow-balanced (zero net mass flow) state is a globally unstable attractor. Hence the state cannot be reached for any constant applied field. To counter the

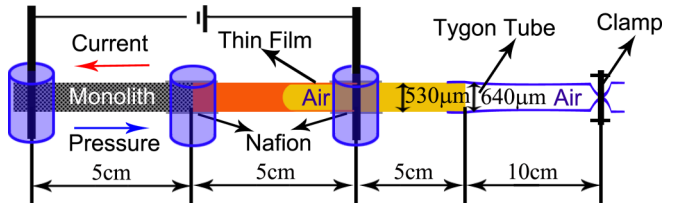


FIG. 1. Schematic of experimental setup.

monolith electro-osmotic flow, a pressure gradient builds up slowly towards the right, corresponding to the negative gauge pressure of the expanding bubble. The large hydrodynamic resistance of the monolith to pressure-driven back flow necessitates a large pressure gradient, hence a prolonged bubble advance, to approach flow balance. This prolonged dewetting significantly displaces the meniscus, thins the film around the bubble, and triggers a delayed film rupture despite the long capillary-viscous drainage time [13]. This rupture breaks the circuit and suppresses electro-osmosis such that the bubble now recedes until the rupture is repaired, initiating and sustaining oscillations under properly biased voltages. Thus oscillations about this unstable zero-flow state are driven by competition between electro-osmotic and pressure-driven flows, with hysteretic switching provided by the dewetting-wetting dynamics of the rupture. The two flow states are reminiscent of Teorell's theory and this relatively unexplored mechanism may be analogous to mechanical stretching of the gating protein by the flow fields or actual flows that displace the meniscus between two phases in an ion channel [6]. However, only a single external gradient is necessary.

## II. METHOD

As shown in Fig. 1, a 5 cm glass capillary (ID 530  $\mu\text{m}$ , OD 660  $\mu\text{m}$ ) filled with a monolith is connected sequentially with two empty 5 cm capillaries by Nafion tubing. The end of the capillary is connected to a 10 cm Tygon tubing (ID 640  $\mu\text{m}$ ). Three reservoirs are located at the beginning of the monolith capillary and at the two Nafion junctions. All tubes in contact with capillaries and two rightmost reservoirs are sealed with UV glue to make the system to the right of the monolith airtight, thus allowing development of internal pressure gradients. The fabrication details of the monolith by solgel chemistry can be found in literature [34]. The membrane monolith pore size is estimated to be about 3.5  $\mu\text{m}$  and it is hence not strongly ion selective. Briefly, the capillary is prewashed with DI water and 1 M sodium hydroxide for 30 min, respectively. After putting it in an oven at 40  $^{\circ}\text{C}$  overnight to activate the surface sites, it is again washed with 0.1 M hydrochloride, DI water, and acetone for 30 min each and dried at 180  $^{\circ}\text{C}$ . A solution of 54 mg polyethylene glycol (PEG), 500  $\mu\text{L}$  0.01 M acetic acid, and 200  $\mu\text{L}$  tetramethoxysilane (TMOS) is mixed with a stir bar in an ice bath for 30 min. The solution is then introduced to the capillary and put in an oven for 40  $^{\circ}\text{C}$  for 24 h with both ends sealed with Teflon tape. It is then washed with DI water and 0.2 M ammonia hydroxide and put in the oven for another 24 h. Finally, the capillary is heated with programmed temperature changing from 40 to 300  $^{\circ}\text{C}$  at a rate of 1  $^{\circ}\text{C}/\text{min}$  and soaked at 80, 120, 180, and 300  $^{\circ}\text{C}$  for 4 h, respectively.

The monolith is prewetted with water with the Tygon tube unclamped. An electrical field across the first two reservoirs is applied to drive liquid into the second capillary. The Tygon tube is then sealed with a clamp to close the left side of the system. Finally, a constant negative electric field is applied across the first and third reservoir to begin the experiments. Oscillations are observed for a wide range of voltages; for positive fields, no oscillations are observed as the system has a single, stable state.

### III. RESULTS AND DISCUSSION

The time series in Fig. 2 shows quasiperiodic oscillations across an applied voltage range of 1 kV; corresponding phase portraits and power spectra are shown in Figs. 3 and 4, respectively. At low voltage (1.5 kV), both the electro-osmotic and pressure-driven flow are relatively small and oscillations are observed with a frequency distribution about a slow ( $\sim 0.02$  Hz) peak. At intermediate voltage (2 kV), the period becomes shorter ( $\sim 10$  s), with a corresponding shift in peak, broadening of the spectrum, and increase in density of phase trajectories about both off and on states. Visual observation indeed indicates rupturing events in the film (see Supplementary Material [35]; a representative 100 s video is provided for each voltage, showing a rapid recoil of the meniscus after the rupture event.). We are unable to image the actual film rupture but such rupturing of a receding meniscus has been studied extensively [13]. However, at high voltage (2.5 kV), the response becomes more irregular, and the bubble stays at the same location during long quasisteady intervals as shown in the video [35] implying nearly stable balance of the pressure-driven flow and electro-osmotic flow in one state. The transition to intermittent, flickerlike oscillations, reflected by the fluctuations of the stationary meniscus, has a classical  $1/f$  power spectrum [36] [see Fig. 4(c)]. The accompanying trajectories still possess two distinct off-on states, though the on state appears much more stable, with slower fluctuations.

To better understand the proposed mechanism for oscillations, we examine the on (high-current-electroosmotic-dominant flow) and off states (low-current-pressure-dominant flow) for the 2.0 kV case in detail. The period plotted against

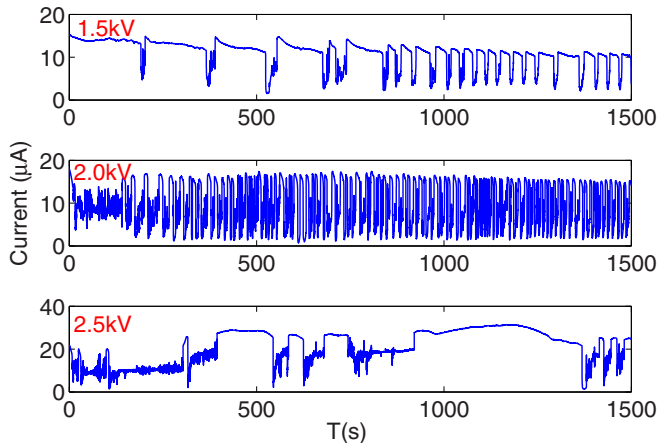


FIG. 2. Time series of current oscillation at different voltages.

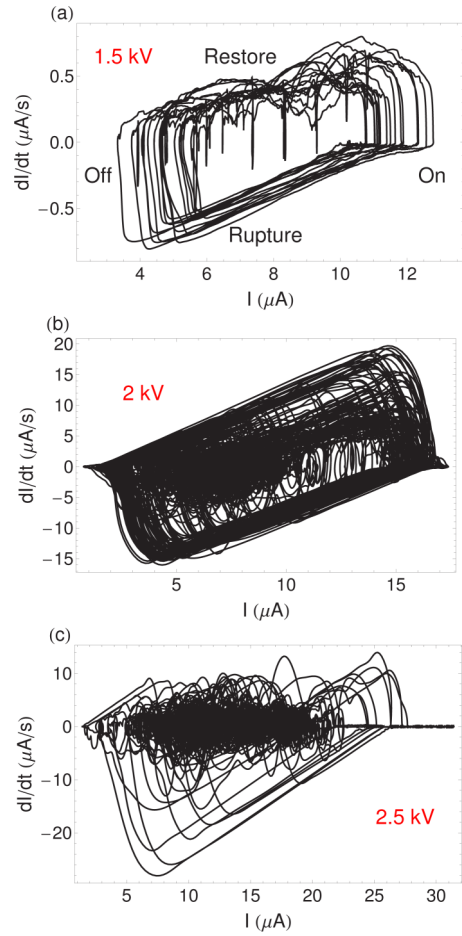


FIG. 3. Phase portraits for the three applied voltages. These are obtained from the time-series data with exponential moving averaging used to filter out high-frequency components for clarity.

the meniscus position amplitude is shown in Fig. 6 [35]. Prior to application of the voltage, the effective bubble length is estimated from the relative inner diameters of the Tygon tube and glass capillary,  $L_0 = 5 + (640/530)^2 \times 10 \approx 20$  cm. Accounting for room-temperature water-air surface tension in the capillary and estimating a (hemispherical) bubble radius of  $\approx 260$   $\mu\text{m}$ , the initial pressure inside the bubble is roughly  $P_0 = 101.87$  kPa, slightly higher than atmospheric pressure. Assuming isothermal volume changes of the bubble with no mass exchange or changes in liquid-vapor equilibrium, and negligible change in curvature of the meniscus or cross section of bubble, for two arbitrary states, the initial and final bubble pressures and displacements due to applied voltage are related by  $P_f L_f = P_i L_i$ . Upon application of voltage, water mass flux is initially from right to left and the bubble expands by about 1 cm, corresponding to a decrease in bubble pressure to about  $P_1 = 97.02$  kPa and a net pressure gradient to the right, opposing the monolith EOF. However, zero mass flux can never be reached in the film around the bubble; EOF thins the film, but the film cannot sustain a pressure gradient to counter it [37]. The thin film around the bubble does however sustain the field and current until rupture (with increasing film resistance), when the flow reverses direction. The bubble then

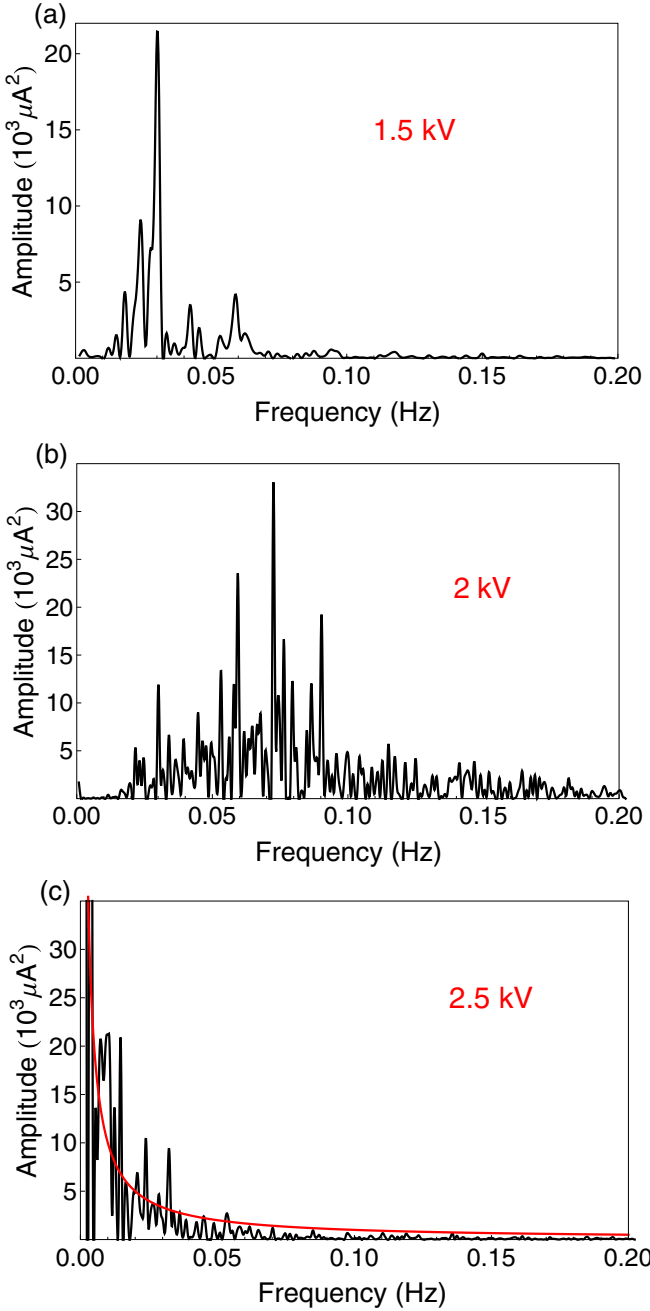


FIG. 4. Power spectra for the three applied voltages obtained from the full, unfiltered time series. The  $1/f$  spectrum is shown in dashed red for 2.5 kV.

recedes until the rupture is repaired. A regular oscillation is hence sustained under a constant dc voltage—a single macroscopic gradient—oscillates with an amplitude around 0.1 cm. This corresponds to pressure fluctuations about  $P_1$  of approximately  $\pm 500$  Pa for bubble lengths between  $L \approx 21.1$  cm and  $L \approx 20.9$  cm (see Fig. 5). Since the hydrodynamic resistance is largest at the monolith, it is the flow rate limiting region. If the monolith is modeled as a bundle of capillaries of radius  $r$  about  $3.5\text{ }\mu\text{m}$  [13] with uniform pressure gradient over each, the averaged pressure-driven velocity contribution is  $U = \Delta P r^2 / 8\eta L_m$ , where  $L_m = 5$  cm. For the on state,

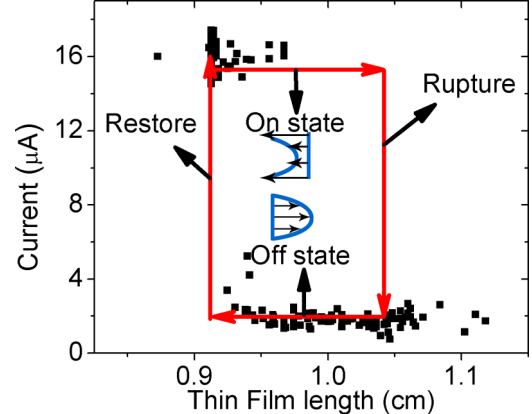


FIG. 5. On-off state switch position for the voltage 2.0 kV oscillation. The different flow states in the monolith are indicated.

this contribution is between 0.13–0.16 mm/s to the right. The EOF velocity is given by  $U = \epsilon\zeta E/\eta$ , estimated with zeta potential  $\zeta = 50$  mV [13]. During the on state, the 0.1 cm (1/10 of the film length) oscillation displacement results in a current change of around  $1\text{ }\mu\text{A}$  (1/16 of the current). Assuming the film thickness remains constant before the rupture event, the thin film resistance is about twice of the sum resistance of the monolith and the capillary filled with electrolyte. So the voltage drop across the monolith is around 0.17–0.18 of the applied voltage; this gives a velocity contribution of about 0.24–0.25 mm/s. Thus the net average velocity in the monolith is about 0.08–0.12 mm/s. If the porosity of the monolith is about 0.27 [34], this corresponds to an average flow velocity in the capillary between about 0.022–0.032 mm/s to the left, compared to the experimental value of 0.16 mm/s observed for the meniscus, as seen in Fig. 6. In the off state, the field across the monolith is estimated to be reduced by about 1/8 from Fig. 5, with a corresponding EOF velocity of about 0.03 mm/s to the right in the monolith. This suggests the net flow velocity in the capillary should be between  $-0.027$  and  $-0.035$  mm/s (to the right), compared to the experimental value of  $-0.10$  mm/s. Both estimated velocities are slower than the measured meniscus velocities, suggesting that a nonuniform thin film and other complicated dynamics, such as concentration polarization [25] and streaming current [38], may be involved.

The dramatic changes in the oscillation periods and spectral shape across 2 kV, as evidenced in Figs. 2 and 4, suggest distinct mechanisms are at play at different voltages. Yet, the off-state current in Fig. 2 is always around 2 A, independent of the voltage. The  $1/f$  dynamics at 2.5 kV is from a nearly stationary bubble with intermittent fluctuations at the meniscus that is quite reminiscent of similar  $1/f$  stick-slip receding contact line dynamics [39], with the robust flow around the nearly stationary bubble rendering the film dynamics near its meniscus similar to that of a receding contact line. The rupturing dynamics and the intense Ohmic heating can produce other dynamics that may be responsible for the two time scales evident at 1.5 and 2.0 kV. However, while all three mechanisms can rupture microscopic films, there remains a continuous nanoscale film, first predicted by de Gennes, at the surface because of van der Waals disjoining forces [13].

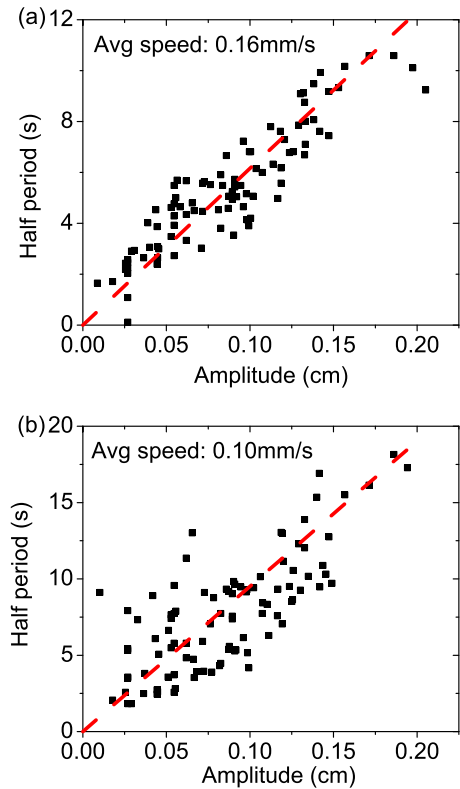


FIG. 6. Correlation between half period and meniscus fluctuation amplitude for the on (a) and off (b) states for oscillation at 2.0 kV. A linear fit is used for the velocity,  $A = vt$ , where  $A$ ,  $v$ ,  $t$  are the amplitude, velocity, and period, respectively. For each set of data  $(A_i, t_i)$ , the fitted velocity is  $v = \sum A_i t_i / \sum t_i^2$  to minimize error.

This film is roughly 10 to 100 nm in thickness, depending on the surface roughness or heterogeneity but not on the voltage. This universal nanofilm that never ruptures may explain the invariant 2  $\mu\text{A}$  current at the off state and the roughly 1/8 ratio of the off-state and on-state current over the voltage range studied.

#### IV. CONCLUSIONS

In summary, ion and mass flux oscillations can indeed be induced with a single macroscopic potential gradient, with hysteretic meniscus wetting-dewetting dynamics driven by the two flow states providing the two distinct states bridged by the oscillations. A switching mechanism between the two states is provided by the delayed film rupture and the bubble expansion is to generate a negative pressure to create a pressure-driven back flow and achieve zero mass flux in the monolith. Although a macroscopic pressure gradient opposite to the potential gradient is not applied, it is generated internally by the monolith as it approaches zero mass flow in the monolith. This feedback hence replaces the other gradient in Teorell's theory and renders the oscillations very robust. The period of the system is strongly dependent on the surface charge and zeta potential but the oscillations appear under all voltages in the proper direction. The film rupture is analogous to mechanical protein collapse into a globule—driven by van der Waals forces for the former and by hydrophobic attraction for the latter. The potential drop across the membrane is about a thousand times smaller in a real ion channel but so is the longitudinal length scale. Hence the electric field, the electro-osmotic velocity, and the oscillation time scales may be comparable. (The regular oscillations at 2.0 kV for Fig. 2 are about 10 s.) Binding of ligands on neurotransmitter gated ion channels are known to activate ion current pulses and oscillations. Similarly, binding of charged or large blocking neutral molecules onto the monolith will change the electro-osmotic flow or pressure-driven backflow, thus triggering the oscillation, changing the frequency spectrum of—or possibly altering the transition voltage to—the 1/f state [36]. Furthermore, the complexities of the meniscus dynamics, especially when accounting for joule heating of the film, may provide an example of a noise-driven state transition [17]. We hence propose this artificial system to sustain robust ion current oscillation with a single external field to be a good biomimetic model for ion current oscillations in an ion channel. Lastly, because of the potential for sensitivity of the 1/f state to adsorption events, such oscillators offer a possible mechanism for molecular detection.

- 
- [1] L. Onsager, *Phys. Rev.* **37**, 405 (1931); **38**, 2265 (1931).
  - [2] J. Keener and J. Sneyd, *Mathematical Physiology* (Springer-Verlag, New York, 1998).
  - [3] A. Mielke, D. Renger, and M. Peletier, *Journal of Non-Equilibrium Thermodynamics* **41**, 141 (2016).
  - [4] A. Revil and P. Leroy, *J. Geophys. Res.: Solid Earth* **109**, B03208 (2004).
  - [5] C. Gonzalez-Fernandez, J. Bruque, F. Gonzalez-Caballero, and A. Hayas, *J. Non-Equilib. Thermodyn.* **9**, 147 (1984).
  - [6] P.-Y. Hsiao, Y.-F. Wei, and H.-C. Chang, *Soft Matter* **7**, 1207 (2011); S. Wang, H.-C. Chang, and Y. Zhu, *Macromolecules* **43**, 7402 (2010).
  - [7] O. Beckstein, P. C. Biggin, and M. S. P. Sansom, *J. Phys. Chem. B* **105**, 12902 (2001); O. Beckstein and M. S. P. Sansom, *Proc. Natl. Acad. Sci. (USA)* **100**, 7063 (2003).
  - [8] S. Khademi, J. O'Connell, J. Remis, Y. Robles-Colmenares, L. J. W. Miercke, and R. M. Stroud, *Science* **305**, 1587 (2004).
  - [9] W. B. Inwood, J. A. Hall, K.-S. Kim, R. Fong, and S. Kustu, *Genetics* **183**, 1341 (2009).
  - [10] L. S. King, D. Kozono, and P. Agre, *Nat. Rev. Mol. Cell Biol.* **5**, 687 (2004).
  - [11] E. A. C. MacRobbie, *Biol. Rev.* **46**, 429 (1971).
  - [12] L.-Q. Gu, S. Cheley, and H. Bayley, *Proc. Natl. Acad. Sci. (USA)* **100**, 15498 (2003).
  - [13] R. V. Craster and O. K. Matar, *Rev. Mod. Phys.* **81**, 1131 (2009).
  - [14] D. Taller, D. B. Go, and H.-C. Chang, *Phys. Rev. Lett.* **109**, 224301 (2012).
  - [15] I. V. Kuchin, O. K. Matar, R. V. Craster, and V. M. Starov, *Soft Matter* **10**, 6024 (2014).

- [16] L. Y. Yeo, R. V. Craster, and O. K. Matar, *Phys. Rev. E* **67**, 056315 (2003).
- [17] M. Pradas, D. Tseluiko, S. Kalliadasis, D. T. Papageorgiou, and G. A. Pavliotis, *Phys. Rev. Lett.* **106**, 060602 (2011).
- [18] T. Teorell, *Discuss. Faraday Soc.* **21**, 9 (1956); *J. Gen. Physiol.* **42**, 831 (1959); **42**, 847 (1959).
- [19] P. Meares and K. R. Page, *Philos. Trans. R. Soc. A* **272**, 1 (1972).
- [20] P. Meares and K. R. Page, *Proc. R. Soc. A* **339**, 513 (1974).
- [21] Y. Kobatake and H. Fujita, *J. Chem. Phys.* **40**, 2212 (1964); **40**, 2219 (1964).
- [22] I. Rubinstein, *Electro-Diffusion of Ions* (Society for Industrial and Applied Mathematics, Philadelphia, 1990).
- [23] V. Pastushenko, *Bioelectrochem. Bioenerget.* **43**, 143 (1997).
- [24] V. Pastushenko, *Electrophoresis* **28**, 683 (2007).
- [25] R. Abu-Rjal, L. Prigozhin, I. Rubinstein, and B. Zaltzman, *Phys. Rev. E* **92**, 022305 (2015).
- [26] Y. Yan, L. Wang, J. Xue, and H.-C. Chang, *J. Chem. Phys.* **138**, 044706 (2013).
- [27] A. J. Storm, J. H. Chen, H. W. Zandbergen, and C. Dekker, *Phys. Rev. E* **71**, 051903 (2005); M. Mihovilovic, N. Hagerty, and D. Stein, *Phys. Rev. Lett.* **110**, 028102 (2013); I. Vlassiouk, T. R. Kozel, and Z. S. Siwy, *J. Am. Chem. Soc.* **131**, 8211 (2009); S. Senapati, S. Basuray, Z. Slouka, L.-J. Cheng, and H.-C. Chang, *Top. Curr. Chem.* **304**, 153 (2011).
- [28] J. N. A. Matthews, *Phys. Today* **65**, 29 (2012).
- [29] S. M. Rubinstein, G. Manukyan, A. Staicu, I. Rubinstein, B. Zaltzman, R. G. H. Lammertink, F. Mugele, and M. Wessling, *Phys. Rev. Lett.* **101**, 236101 (2008); G. Yossifon and H.-C. Chang, *ibid.* **101**, 254501 (2008); H.-C. Chang, G. Yossifon, and E. A. Demekhin, *Annu. Rev. Fluid Mech.* **44**, 401 (2012).
- [30] J. Schiffbauer and G. Yossifon, *Phys. Rev. E* **86**, 056309 (2012).
- [31] Z. Siwy and A. Fulniński, *Phys. Rev. Lett.* **89**, 198103 (2002); C. Wei, A. J. Bard, and S. W. Feldberg, *Anal. Chem.* **69**, 4627 (1997); D. Momotenko and H. H. Girault, *J. Am. Chem. Soc.* **133**, 14496 (2011).
- [32] L.-J. Cheng and H.-C. Chang, *Biomicrofluidics* **5**, 046502 (2011); Z. Slouka, S. Senapati, and H.-C. Chang, *Annu. Rev. Anal. Chem.* **7**, 317 (2014).
- [33] M. R. Powell, M. Sullivan, I. Vlassiouk, D. Constantin, O. Sudre, C. C. Martens, R. S. Eisenberg, and Z. S. Siwy, *Nat. Nanotechnol.* **3**, 51 (2008); B. Hyland, Z. S. Siwy, and C. C. Martens, *J. Phys. Chem. Lett.* **6**, 1800 (2015).
- [34] P. Wang, Z. Chen, and H.-C. Chang, *Electrophoresis* **27**, 3964 (2006); *Sensor. Actuat. B-Chem.* **113**, 500 (2006); Z. Chen, P. Wang, and H.-C. Chang, *Anal. Bioanal. Chem.* **382**, 817 (2005).
- [35] See Supplemental Material at <http://link.aps.org/supplemental/10.1103/PhysRevE.94.022613> for oscillation videos of the meniscus.
- [36] W. Schottky, *Phys. Rev.* **28**, 74 (1926).
- [37] P. Takhistov, A. Indeikina, and H.-C. Chang, *Phys. Fluids* **14**, 1 (2002).
- [38] J. Yang, F. Lu, L. W. Kostiuk, and D. Y. Kwok, *J. Micromech. Microeng.* **13**, 963 (2003); Y. Yan, Q. Sheng, C. Wang, J. Xue, and H.-C. Chang, *J. Phys. Chem. C* **117**, 8050 (2013).
- [39] S. Maheshwari, L. Zhang, Y. Zhu, and H.-C. Chang, *Phys. Rev. Lett.* **100**, 044503 (2008).